On the interplay effects with proton scanning beams in stage III lung cancer

Yupeng Li
Department of Radiation Physics, The University of Texas MD Anderson Cancer Center, Houston, Texas 77030 and Applied Research, Varian Medical Systems, Palo Alto, California 94304

Laleh Kardar
Department of Industrial Engineering, The University of Houston, Houston, Texas 77204

Xiaoqiang Li and Heng Li
Department of Radiation Physics, The University of Texas MD Anderson Cancer Center, Houston, Texas 77030

Wenhua Cao
Department of Radiation Physics, The University of Texas MD Anderson Cancer Center, Houston, Texas 77030 and Department of Industrial Engineering, The University of Houston, Houston, Texas 77204

Joe Y. Chang
Department of Radiation Oncology, The University of Texas MD Anderson Cancer Center, Houston, Texas 77030

Li Liao
Department of Industrial Engineering, The University of Houston, Houston, Texas 77204

Ronald X. Zhu, Narayan Sahoo, and Michael Gillin
Department of Radiation Physics, The University of Texas MD Anderson Cancer Center, Houston, Texas 77030

Zhongxing Liao, Ritsuko Komaki, and James D. Cox
Department of Radiation Oncology, The University of Texas MD Anderson Cancer Center, Houston, Texas 77030

Gino Lim
Department of Industrial Engineering, The University of Houston, Houston, Texas 77204

Xiaodong Zhang[a)]
Department of Radiation Physics, The University of Texas MD Anderson Cancer Center, Houston, Texas 77030

(Received 25 July 2013; revised 10 December 2013; accepted for publication 30 December 2013; published 23 January 2014)

Purpose: To assess the dosimetric impact of interplay between spot-scanning proton beam and respiratory motion in intensity-modulated proton therapy (IMPT) for stage III lung cancer.
Methods: Eleven patients were sampled from 112 patients with stage III nonsmall cell lung cancer to well represent the distribution of 112 patients in terms of target size and motion. Clinical target volumes (CTVs) and planning target volumes (PTVs) were defined according to the authors' clinical protocol. Uniform and realistic breathing patterns were considered along with regular- and hypofractionation scenarios. The dose contributed by a spot was fully calculated on the computed tomography (CT) images corresponding to the respiratory phase that the spot is delivered, and then accumulated to the reference phase of the 4DCT to generate the dynamic dose that provides an estimation of what might be delivered under the influence of interplay effect. The dynamic dose distributions at different numbers of fractions were compared with the corresponding 4D composite dose which is the equally weighted average of the doses, respectively, computed on respiratory phases of a 4DCT image set.
Results: Under regular fractionation, the average and maximum differences in CTV coverage between the 4D composite and dynamic doses after delivery of all 35 fractions were no more than 0.2% and 0.9%, respectively. The maximum differences between the two dose distributions for the maximum dose to the spinal cord, heart V40, esophagus V55, and lung V20 were 1.2 Gy, 0.1%, 0.8%, and 0.4%, respectively. Although relatively large differences in single fraction, correlated with small CTVs relative to motions, were observed, the authors' biological response calculations suggested that this interfractional dose variation may have limited biological impact. Assuming a hypofractionation scenario, the differences between the 4D composite and dynamic doses were well confined even for single fraction.
Conclusions: Despite the presence of interplay effect, the delivered dose may be reliably estimated using the 4D composite dose. In general the interplay effect may not be a primary concern with IMPT for lung cancers for the authors' institution. The described interplay analysis tool may be used

to provide additional confidence in treatment delivery. © *2014 American Association of Physicists in Medicine*. [http://dx.doi.org/10.1118/1.4862076]

Key words: interplay, proton scanning, IMPT, lung cancer, respiratory motion

1. INTRODUCTION

Intensity modulated proton therapy (IMPT), typically based on scanning proton beams, provides greater control over dose distributions than the techniques based on collimated broad beams (e.g., the double scattering proton therapy).[1,2] In treatment of lung cancer, IMPT could further increase the dose delivered to the tumor while minimizing that delivered to surrounding healthy organs, such as the lung, esophagus, and spinal cord.[3–5] A dominant concern that hinders the application of IMPT to lung cancers is potential local regions of under- and overdoses resulting from the effect of interplay between proton spot scanning and intrafractional respiratory motion in dose delivery.

A scanning proton beam covers a three-dimensional target volume laterally by sequentially delivering a series of narrow, nearly monoenergetic beams called scanning spots, and longitudinally layer by layer via altering proton energy. In patients with lung cancer, intrafractional motion of tumors and organs is highly correlated with respiration, and the time scales of this motion are at the same level as the spot-scanning processes. Therefore, a scanning spot could be delivered to a location not as planned because the spot "sees" an anatomy that may be quite different from that in the planning computed tomography (CT) images. Consequently, the actual delivered dose may seriously deviate from the nominal dose distribution calculated on the same free-breathing or average CT images with which the treatment plan is designed. This interplay between periodic anatomical changes and beam scanning adds complications in predicting the effects of organ motion on the delivered dose distributions.[6,7]

Bortfeld *et al.*[8] statistically studied interplay effect with dynamic photon beams. They showed that under extreme situations, parts of tumors could be completely missed by irradiation in the presence of respiratory motion. In reality, however, interplay effect may be largely diminished by fractionation and repainting.[8] Also, studies focused on proton scanning beams demonstrated that highly heterogeneous dose distributions are likely, but may be significantly reduced by fractionation and repainting.[6,7] For the spot scanning treatment at the University of Texas MD Anderson Cancer Center (MDACC) Proton Therapy Center, Houston, Texas (PTC-H), we adopted an isolayer repainting style (ILR) in which all planned positions are first visited once by a deliverable spot, then repeated as needed until all planned MUs are delivered before the next energy layer can be initiated.

Use of composite doses or other methods based on four-dimensional (4D) CT images and image registration has been proposed for evaluating the actual delivered dose in the presence of respiratory motion.[9–11] For example, dose calculation may be repeated in each respiratory phase in a 4DCT set, and the doses in different phases are transformed to and averaged on the reference phase to obtain a 4D composite dose. According to previous interplay studies, however, it is necessary that this method be reassessed for evaluating dynamic dose distributions under the influence of interplay effect. It was theoretically shown using a generalized model that the dynamic dose converges to the 4D composite dose in multiple deliveries through fractionation and rescanning despite interplay.[12] Applying what this theoretical derivation suggests to practical clinical settings requires further investigations.

In the present study, we assessed dynamic dose distributions in the presence of interplay effect, taking into account dose fractionation, respiration irregularity, and isolayer repainting with clinically adopted treatment planning procedures and beam-delivery system details at PTC-H. We performed the simulations using our 4D interplay simulation program with 11 patients sampled from 112 patients with stage III nonsmall cell lung cancer previously treated at MDACC. We then compared our simulation results with corresponding nominal and 4D composite doses. Based on the results of this study, we made recommendations that facilitate application of IMPT in the presence of respiratory motion.

2. METHODS AND MATERIALS

2.A. Patient selection

Tumor motion and size were analyzed from 4DCT images of 112 patients with stage III nonsmall cell lung cancer who previously received intensity-modulated x-ray radiation therapy (IMRT) or double scattering proton therapy at MDACC. Their clinical target volumes (CTVs) ranged from 26 to 1360 cc (median, 336 cc), whereas their center-to-center CTV motions (i.e., difference between centers of mass) ranged from 0.2 to 16.6 mm (median, 3.3 mm) (Fig. 1). Of the 112 patients, 31%, 49%, and 20% had target motions ranging from 0 to 2.5 mm, ranging from 2.5 to 5.0 mm, and greater than 5.0 mm, respectively. Eleven patients uniformly representing

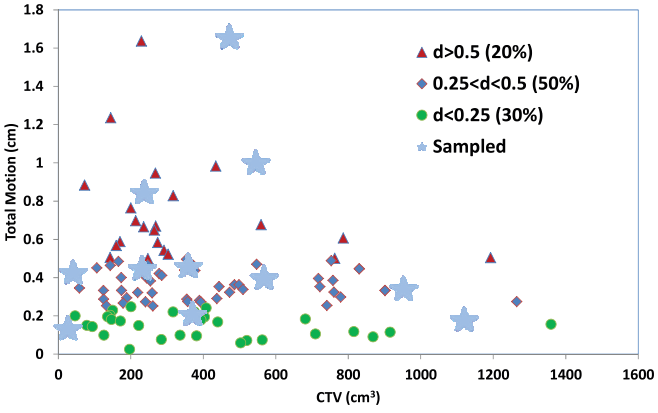

FIG. 1. Eleven patients (stars) were sampled to uniformly represent 112 with stage III nonsmall cell lung cancer.

TABLE I. CTV location, size, and motions.

Patient no.	CTV location	CTV volume (cc)	CTV motion (mm)
1	RM	472.15	16.6
2	RL	545.09	10.0
3	RU	236.84	8.5
4	LM	358.24	4.6
5	RU	230.99	4.5
6	LM	40.83	4.3
7	RU	567.5	4.0
8	RU	952.57	3.4
9	LM	370.44	2.1
10	RU	1119.78	1.8
11	RM	26.17	1.4

Note: R, right; L, left; U, upper; L, lower; and M, middle.

the group in terms of tumor size and motion were selected by using a stratified sampling method on the above three motion categories, and the dynamic doses in these patients were quantitatively analyzed. Table I lists the CTV location, size, and motion for the selected patients.

2.B. Proton spot-scanning system

The beam delivery system (PROBEAT; Hitachi America, Ltd., Tarrytown, NY) used at PTC-H provides discrete spot scanning using a synchrotron.[13] The synchrotron generates a spill of proton beams with the maximum duration of 4.4 s in each acceleration cycle. Switching of energy requires a new spill. Deceleration and acceleration of protons between spills take 2.1 s. Multiple scanning spots with the same energy are delivered within a spill. The full width at half maximum of a scanning spot ranges from 12.8 to 34.3 mm in air at the isocenter as the proton energy varies from 221.8 to 72.5 MeV. The irradiation time per spot is from 1 to 10 ms, depending on spot monitor units (MU). If the spot MU is greater than the maximum allowed value of 0.04, the spot is split into multiple spots, which are delivered through ILR, so that the maximum MU limit is satisfied for each spot (i.e., the spot is deliverable). The interval is about 3 ms between spots within a spill (Fig. 2). At PTC-H, the sequence of spot scans that cover the entire area of an energy layer is repeated as needed until all MUs are delivered at that energy and before the next energy layer can be initiated.

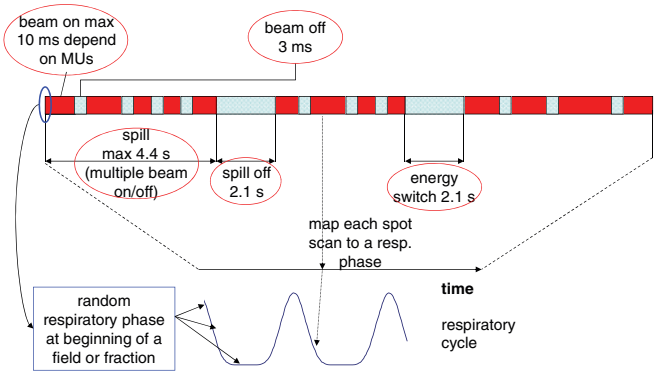

FIG. 2. To simulate interplay effect, time required for each delivery step was tracked, and a respiratory phase was assigned to each spot according to the recorded time stamp.

2.C. 4DCT

4DCT images of the patients included in this study were acquired using a GE LightSpeed 16-slice CT scanner (GE Healthcare, Waukesha, WI) with a cine scanning protocol[14] as part of the radiotherapy planning process. Multiple CT images acquired at each table position were binned retrospectively into multiple phases according to respiratory signals recorded externally using a real-time position management (RPM) system (Varian Medical Systems, Palo Alto, CA). Each respiratory period is divided equally into ten phases T0 to T90 in which T50 corresponds to the exhalation phase. A "demons" deformable image registration algorithm[15] was used to generate three-dimensional deformation vectors that mapped image pixels in different respiratory phases to pixels in the reference phase T50. Using this information, proton doses calculated in different respiratory phases can be accumulated and evaluated in the reference phase, taking into account of breathing-related organ deformations.

2.D. IMPT treatment planning

CTVs were created by expanding corresponding gross tumor volumes (GTV) of primary tumors and diseased lymph nodes by 8 mm. A planning target volume (PTV) was created by expanding 5 mm from the internal target volume (ITV) which was the union of CTVs in phases T0 and T50. Three-field IMPT plans were optimized on average CT images with previously described optimization algorithms[16,17] in an in-house IMPT research system developed and verified at MDACC.[18]

2.E. Simulation of the interplay effect

The tool used for simulation of interplay effect in our study was developed based on a previously implemented dose algorithm.[18] Because proton beams are highly sensitive to anatomical changes, the dose from a spot needs to be fully calculated for its assigned respiratory phase. This tool essentially enables the highly computation-intensive simulations and analysis required for this study with a relatively large number of patients.

Because of the time-dependent nature of the spot scanning process and periodic organ motion, the instant dose delivered by spot j to the dose voxel at (x, y, z) is a function of time, and the total dose from spot j can be described as

$$D_j(x, y, z) = \int_t \dot{D}_j(x, y, z, t)\mathrm{d}t, \quad (1)$$

where $\dot{D}_j(x, y, z, t)$ is the dose rate from spot j at moment t. For photon beams, $\hat{D}_j(x, y, z, t)$ may be sufficiently approximated by $\dot{D}_j(x(t), y(t), z(t), t_0)$, assuming spatial dose shift invariance, in which the point at position (x, y, z) at moment t_0 is moved to position $(x(t), y(t), z(t))$ due to organ

movement. However, the difference between $\dot{D}_j(x, y, z, t)$ and $\dot{D}_j(x(t), y(t), z(t), t_0)$ may no longer be negligible for proton beams, and the dose therefore needs to be recalculated for changed anatomies.

To simulate interplay effect, the time spent in each spot-scanning step (e.g., turning beams on and off, switching energies, starting new spills) was tracked as the scanning process proceeded, and a respiratory phase was assigned to each spot according to the recorded time stamp (Fig. 2). A random respiratory phase was assigned to the beginning of each fraction and field. The maximum duration for a scanning spot of 10 ms was much shorter than each of the ten phases of the respiratory cycle (200–400 ms per phase) in our beam-delivery system settings. $\dot{D}_j(x, y, z, t)$ can be calculated based on the CT images of the respiratory phase corresponding to moment t. With each spot fully calculated for its assigned respiratory phase, doses in different phases from all spots were summed to acquire the dynamic dose distribution in the reference phase using deformation vectors generated by the deformable image registration:

$$D(x, y, z) = \sum_j D_j(x, y, z) = \sum_j (\bar{D}_j(x, y, z, n) \cdot w_j), \quad (2)$$

where $\bar{D}_j(x, y, z, n)$ is the dose rate in Gy/MU calculated in the respiratory phase denoted by n that is assigned to spot j and w_j is the spot weight in MUs.

2.F. Study design

A series of dynamic doses incorporating interplay effects were simulated for regular- and hypofractionation scenarios. A uniform breathing pattern modeled by an asymmetrical sinusoidal function[19] with the period of 4.2 s, and three realistic breathing patterns extracted from patient RPM data with various irregularities, characterized by the standard deviation (SD) in the length of breathing cycles (0.13, 0.46, and 0.93 s), were included in the present study. The calculated dynamic dose distribution was compared with the 4D composite dose distribution in T50.

3. RESULTS

3.A. Regular fractionation

Figure 3(a) shows average differences in the percent CTV covered by prescription 70 Gy between 4D composite and dynamic doses [$V70_{composite}$ (%) − $V70_{dynamic}$ (%)] for all 11 patients. The error bars indicate the maximum and minimum differences. Results for one, five, and ten fractions were normalized in order to be compared with the 4D composite doses around 70 Gy. The average and maximum differences in CTV coverage were no more than 0.2% and 0.9%, respectively, for total 35 fractions. The large spreads up to 6.5% in CTV coverage differences between 4D composite and dynamic doses observed with one fraction resulted mainly from the smallest CTV volumes 26.2, 40.8, and 236.8 cc,

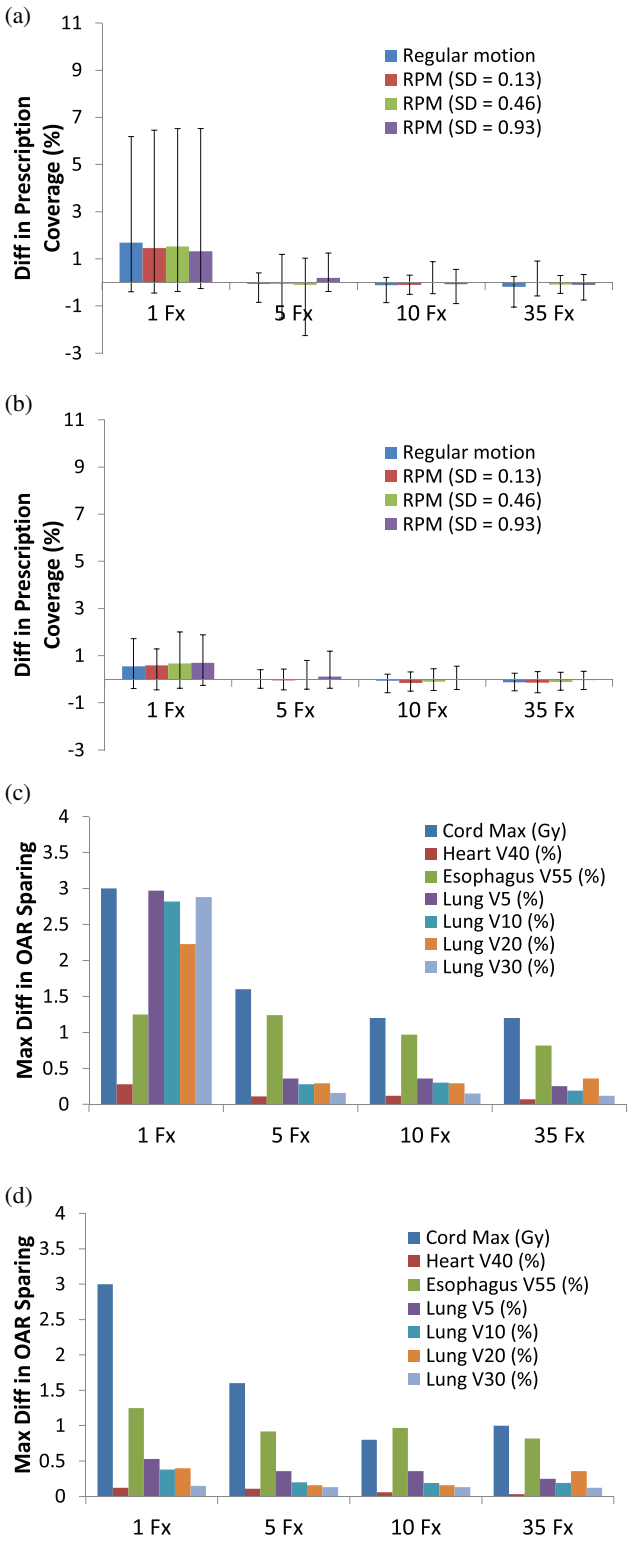

FIG. 3. Between 4D composite and dynamic doses for regular fractionation, average differences in percent CTV covered by prescription in (a) all 11 patients and (b) remaining 8 patients if the smallest CTV in each motion category was excluded. The error bars show the maximum and minimum differences between the two doses. Largest differences of maximum spinal cord doses in Gy, and of heart V40, esophagus V55, lung V5, V10, V20, and V30 in percentage between 4D composite and dynamic dose distributions considering different breathing patterns among (c) all 11 patients, and (d) eight patients if three patients with large CTV motion (>0.8 cm) were excluded.

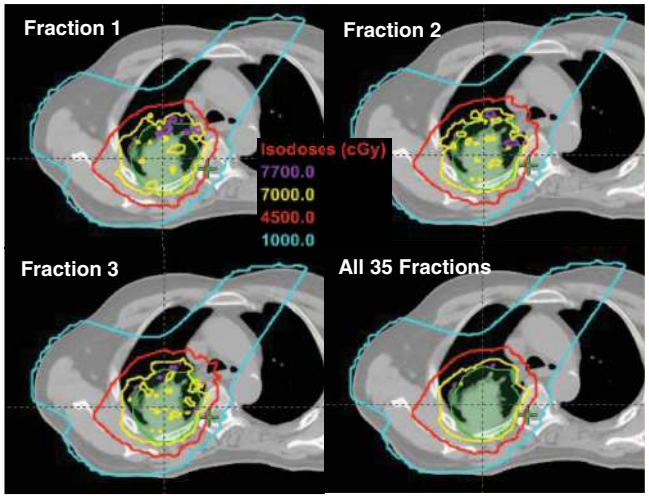

FIG. 4. Nonuniform doses in single fractions were smoothed after all 35 fractions were delivered.

respectively, in the three motion categories. After excluding the three patients, the spreads in one fraction became considerably smaller [Fig. 3(b)]. The average and maximum differences between the 4D composite and dynamic doses for one fraction were less than 0.7% and 2%, respectively, for the remaining eight patients including one with large motion 16.6 mm but a relatively large CTV volume 472 cc. In general, the difference in CTV coverage between the 4D composite and dynamic doses decreased dramatically with as few as five delivered fractions. Figure 4 illustrates how relatively large dose spreads in single fractions were smoothed out after all 35 fractions were delivered.

For certain number of fractions, the absolute differences between 4D composite and dynamic dose distributions were computed for the maximum spinal cord dose, heart V40, esophagus V55, and lung V5, V10, V20, and V30, respectively. Figure 3(c) shows the maximum differences among all 11 patients considering different breathing patterns. For the maximum spinal cord dose, heart V40, esophagus V55, and lung V5, V10, V20, and V30, the maximum differences between the dynamic and 4D composite doses were 3.0 Gy, 0.28%, 1.25%, 2.97%, 2.82%, 2.23%, and 2.88%, respectively, for one fraction. The maximum difference decreased to 1.2 Gy, 0.07%, 0.82%, 0.25%, 0.19%, 0.36%, and 0.12%, respectively, after delivery of all 35 fractions. These maximum dose differences in one fraction improved after we excluded three cases with large target motion (>0.8 cm) from the analysis [Fig. 3(d)]. For the remaining eight patients, the maximum differences between the 4D composite and one-fraction dynamic doses for the spinal cord maximum dose, heart V40, esophagus V55, and lung V5, V10, V20, and V30 became 3 Gy, 0.12%, 1.25%, 0.53%, 0.38%, 0.40%, and 0.15%, respectively.

3.B. Hypofractionation

We also performed hypofractionation simulations with a prescribed dose of 50 Gy delivered in ten fractions for the

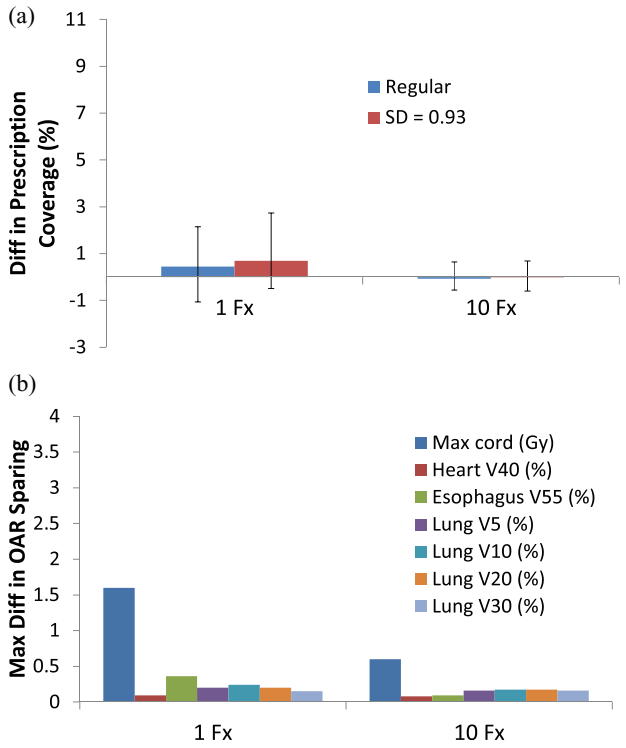

FIG. 5. Differences between 4D composite and dynamic doses under a hypofractionation scenario in all 11 patients. (a) Average differences in percent CTV covered by prescription, where the error bars indicate the maximum and minimum differences. (b) The maximum differences in critical organ sparing.

uniform breathing pattern and the realistic pattern with SD 0.93 s. Figure 5(a) shows the average differences in the percent CTV covered by 50 Gy between 4D composite and dynamic doses [$V50_{composite}$ (%) − $V50_{dynamic}$ (%)] in the 11 patients. Again, the error bars indicate the maximum and minimum differences. The one-fraction results were normalized to 50 Gy in order to be compared to the 4D composite doses. The average and maximum differences were about 0.7% and 2.7%, respectively, for the renormalized one-fraction dose. Comparing these results with regular-fractionation results regardless of target volume and motion, the differences decreased with the increased dose and delivery time per fraction, which in turn corresponded to increased probability of spreading the dose evenly throughout all respiratory phases. Because the maximum MU that can be delivered by a spot is limited, more ILRs would be required with higher dose per fraction in hypofractionation. After the total dose of 50 Gy was delivered in ten fractions, the average and maximum differences in CTV coverage between the 4D composite and dynamic doses were within 0.1% and 0.7%, respectively.

Figure 5(b) shows the maximum differences in dose received by normal organs between the 4D composite and dynamic doses among all 11 patients, with different breathing patterns, motions, and CTV volumes. For one-fraction results, the maximum difference in normal organ doses was 1.6 Gy and 0.4%, respectively, for spinal cord maximum dose and esophagus V55. After delivery of all ten fractions, the maximum differences were about 0.6 Gy and 0.1%, respectively. The maximum differences in doses received by the heart V40,

and lung V5, V10, V20, and V30, were all less than 0.3% for one fraction and 0.2% for ten fractions.

3.C. Biological effects of interfractional dose variation

We assessed the biological responses of two patients in terms of tumor-control probability (TCP) under the interplay effect for CTVs using Källman's S-model.[20] This model can be used to calculate biological responses for nonuniform dose delivery in fractionated therapy. The first patient showed large differences in CTV coverage between the renormalized one-fraction dynamic and 4D composite doses of up to 6.5%. The parameters D50 = 49.2 Gy, $\gamma = 1$, and $\alpha/\beta = 10$ were used for TCP calculation, where D50 was the dose of 50% response, γ was the normalized dose–response gradient, and α and β were the linear quadratic cell-survival parameters. We compared the response of the 4D composite dose assuming equal doses per fraction and the combined responses of, respectively, calculated one-fraction dynamic doses. We observed that dose variations among fractions resulting from the interplay effect did not cause dramatic variations in TCP. The TCP was 82.5% for equal fractional doses and 80.8% for nonuniform fractional doses in the first patient, whereas it was 84.6% under both scenarios in the second patient.

4. DISCUSSIONS

Based on general conclusions from previous investigations, a thorough study targeting the specific clinical planning and treatment process, and machine specifications is necessary to quantify clinical impact of interplay effect at this early stage of applying scanning proton beam especially IMPT on lung cancer radiotherapy. Although dosimetric advantages of IMPT have been established for some time,[5] we only recently started treating lung cancer using IMPT owing to progresses in robust optimization[21] and this study. Our major conclusion that efficacy of IMPT may not be affected by interplay effect considering fractionation and ILR is consistent with a very recent study.[22] In addition, our study also indicated that center-to-center motion alone may not be a good measure of the effect. We observed that situations with motion less than 0.5 cm but small tumor size led to relative large uncertainties caused by interplay effects in single fraction. Based on this study, we are also cautiously extending current IMPT treatment of lung cancer to those patients with motion larger than 0.5 cm with mandated interplay analysis using the tool described here. Despite the positive findings, readers should be cautioned that the above observation was based on the spot sizes that may be large relative to those adopted by other centers, and meanwhile the tumor motion beyond the range included in this study could be encountered. Previous studies have shown that proton dose could be enormously impacted by the interplay effect for large tumor motions around or larger than 10 mm and relatively small spot sizes.[6,22,23] Therefore, we strongly urge that institution-specific study may be necessary for establishing and verifying institution-specific treatment procedures.

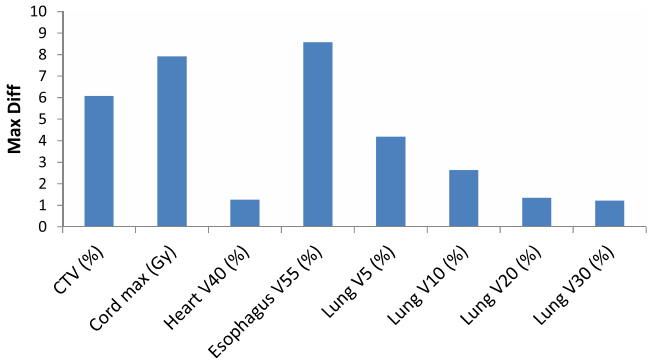

FIG. 6. The maximum differences in dose–volume data between nominal and 4D composite doses in the 11 patients.

Plan evaluation using nominal doses remains a common practice. However, the delivered dose almost always deviates from the designed nominal dose in presence of organ motion and anatomical heterogeneity in proton therapy. The 4D composite dose is a commonly recommended approach for evaluating respiratory motion effects. As shown in Fig. 6, there may be large differences in dose–volume statistics between the nominal and 4D composite doses. Based on the results of this study, we recommend that an IMPT treatment plan be carefully evaluated for cases with respiratory motion using the 4D composite dose distribution. Because spatial dose distributions are highly sensitive to changes of heterogeneous patient anatomy for proton beams, the dose in proton therapy needs to be calculated *ab initio* for each respiration phase to accurately account for the effect of organ motion. Each breathing phase of the 4D CT in this study is an averaged image reconstruction during a 0.5 s period. Because the anatomical changes were not modeled within each phase, the accuracy of our interplay simulation was limited by the temporal length of breathing phases. Considering that respiratory cycles are typically of the order of seconds, however, the simulation based on the phase length of 0.5 s is expected to be sufficient for our clinical needs. Routine use of this time-consuming dose evaluation process for every patient may be impractical. However, the interplay analysis tool described in this study may still be used to validate selected proton scanning plans especially for cases with large respiratory motion and/or small target volumes. Due to time limitation, we only performed fraction-by-fraction interplay simulations, and calculated the overall TCP for two patients in this study. As part of future work, we plan to perform this thorough assessment on a number of patients to establish the confidence that large impact on TCP may be in general unlikely. It may need to be repeated for some special and extreme cases.

Respiratory gating would help mitigate the effect of respiratory motion. However, this would inevitably require holding extra beam time outside duty cycles and cause a good portion of energized protons to be discarded especially with a synchrotron. The present study revealed that respiration-induced tumor motion was no greater than 0.5 cm in the majority of our patients (~77%). Similar motion scale has been reported in Refs. 24 and 25. Even with tumor motion greater than 0.5 cm, our study showed that the final delivered dose may

still be reliably represented using 4D composite doses. IMPT may be delivered efficiently and safely without involving more complicated techniques or extra beam times, which may further increase already high cost of proton therapy. 4D interplay analyses could also be selectively performed for additional assurance.

5. CONCLUSIONS

Based on our study of 11 patients uniformly sampled from 112 patients with stage III nonsmall cell lung cancer, the dose delivered in multiple fractions and ILRs in the presence of interplay effect (dynamic dose) can be estimated with good confidence using 4D composite dose distributions for our and similar beam-delivery system parameters. Relatively large differences between the 4D composite and dynamic doses may present in single fraction with regular fractionation, correlated primarily with relatively small CTVs, although our biological response calculations suggested that this interfractional dose variation may have limited biological impact. If assuming a hypofractionation scenario with a high dose per fraction, the impact of interplay effect was even less pronounced than that with regular fractionation. Therefore, the interplay effect may not be a primary concern in general when applying IMPT in treating lung cancers with the beam delivery system and clinical procedures at PTC-H. However, we recommend that 4D composite dose distributions be carefully evaluated and attentions be paid to small CTV size and large motion. The 4D interplay analysis tool described here can be used to provide additional confidence in treatment planning.

ACKNOWLEDGMENTS

The authors thank Lei Dong, Peter Balter, Enzhuo Quan, and Radhe Mohan for informative discussions and Donald Norwood from the Department of Scientific Publication at the University of Texas MD Anderson Cancer Center for the kind assistance in editing. This research is supported in part by the MD Anderson Cancer Center Support Grant No. CA016672 and a grant from Varian Medical System. The authors report no conflicts of interest in conducting the research.

[a]Author to whom correspondence should be addressed. Electronic mail: xizhang@mdanderson.org; Telephone: (713) 563-2533; Fax: (713) 563-1521.

[1]A. Lomax, "Intensity modulation methods for proton radiotherapy," Phys. Med. Biol. **44**, 185–205 (1999).
[2]A. T. Berman, B. K. K. Teo, D. Dolney, S. Swisher-McClure, K. Shahnazi, S. Both, and R. Rengan, "An in-silico comparison of proton beam and IMRT for postoperative radiotherapy in completely resected stage IIIA non-small cell lung cancer," Radiat. Oncol. **8**, 144 (2013).
[3]D. Georg, M. Hillbrand, M. Stock, K. Dieckmann, and R. Potter, "Can protons improve SBRT for lung lesions? Dosimetric considerations," Radiother. Oncol. **88**, 368–375 (2008).
[4]R. C. Nichols, R. H. Henderson, S. Huh, S. Flampouri, Z. F. Li, A. A. Bajwa, H. J. D'Agostino, D. C. Pham, N. P. Mendenhall, and B. S. Hoppe, "Proton therapy for lung cancer," Thorac. Cancer **3**, 109–116 (2012).
[5]X. Zhang, Y. Li, X. Pan, X. Li, R. Mohan, R. Komaki, J. D. Cox, and J. Y. Chang, "Intensity-modulated proton therapy reduces the dose to normal tissue compared with intensity-modulated radiation therapy or passive scattering proton therapy and enables individualized radical radiotherapy for extensive stage IIIB non-small-cell lung cancer: A virtual clinical study," Int. J. Radiat. Oncol., Biol., Phys. **77**, 357–366 (2010).
[6]K. M. Kraus, E. Heath, and U. Oelfke, "Dosimetric consequences of tumour motion due to respiration for a scanned proton beam," Phys. Med. Biol. **56**, 6563–6581 (2011).
[7]J. Lambert, N. Suchowerska, D. R. McKenzie, and M. Jackson, "Intrafractional motion during proton beam scanning," Phys. Med. Biol. **50**, 4853–4862 (2005).
[8]T. Bortfeld, K. Jokivarsi, M. Goitein, J. Kung, and S. B. Jiang, "Effects of intra-fraction motion on IMRT dose delivery: Statistical analysis and simulation," Phys. Med. Biol. **47**, 2203–2220 (2002).
[9]M. Engelsman, E. Rietzel, and H. M. Kooy, "Four-dimensional proton treatment planning for lung tumors," Int. J. Radiat. Oncol., Biol., Phys. **64**, 1589–1595 (2006).
[10]N. Wang, B. Patyal, A. Ghebremedhin, and D. Bush, "Evaluation and comparison of New 4DCT based strategies for proton treatment planning for lung tumors," Radiat. Oncol. **8**, 73 (2013).
[11]Y. Kang, X. Zhang, J. Y. Chang, H. Wang, X. Wei, Z. Liao, R. Komaki, J. D. Cox, P. A. Balter, H. Liu, X. R. Zhu, R. Mohan, and L. Dong, "4D Proton treatment planning strategy for mobile lung tumors," Int. J. Radiat. Oncol., Biol., Phys. **67**, 906–914 (2007).
[12]H. Li, Y. Li, X. Zhang, X. Li, W. Liu, M. T. Gillin, and X. R. Zhu, "Dynamically accumulated dose and 4D accumulated dose for moving tumors," Med. Phys. **39**, 7359–7367 (2012).
[13]M. T. Gillin, N. Sahoo, M. Bues, G. Ciangaru, G. Sawakuchi, F. Poenisch, B. Arjomandy, C. Martin, U. Titt, K. Suzuki, A. R. Smith, and X. R. Zhu, "Commissioning of the discrete spot scanning proton beam delivery system at the University of Texas MD Anderson Cancer Center, Proton Therapy Center, Houston," Med. Phys. **37**, 154–163 (2010).
[14]T. Pan, T. Y. Lee, E. Rietzel, and G. T. Y. Chen, "4D-CT imaging of a volume influenced by respiratory motion on multi-slice CT," Med. Phys. **31**, 333–340 (2004).
[15]H. Wang, L. Dong, J. O'Daniel, R. Mohan, A. S. Garden, K. K. Ang, D. A. Kuban, M. Bonnen, J. Y. Chang, and R. Cheung, "Validation of an accelerated 'demons' algorithm for deformable image registration in radiation therapy," Phys. Med. Biol. **50**, 2887–2905 (2005).
[16]Y. Li, X. Zhang, and R. Mohan, "An efficient dose calculation strategy for intensity modulated proton therapy," Phys. Med. Biol. **56**, N71–N84 (2011).
[17]X. Zhang, X. Li, E. M. Quan, X. Pan, and Y. Li, "A methodology for automatic intensity-modulated radiation treatment planning for lung cancer," Phys. Med. Biol. **56**, 3873–3893 (2011).
[18]Y. Li, R. X. Zhu, N. Sahoo, A. Anand, and X. D. Zhang, "Beyond Gaussians: A study of single-spot modeling for scanning proton dose calculation," Phys. Med. Biol. **57**, 983–997 (2012).
[19]A. E. Lujan, E. W. Larsen, J. M. Balter, and R. K. Ten Haken, "A method for incorporating organ motion due to breathing into 3D dose calculations," Med. Phys. **26**, 715–720 (1999).
[20]P. Kallman, A. Agren, and A. Brahme, "Tumor and normal tissue response to fractionated non-uniform dose delivery," Int. J. Radiat. Biol. **62**, 249–262 (1992).
[21]W. Liu, X. Zhang, Y. Li, and R. Mohan, "Robust optimization of intensity modulated proton therapy," Med. Phys. **39**, 1079–1091 (2012).
[22]C. Grassberger, S. Dowdell, A. Lomax, G. Sharp, J. Shackleford, N. Choi, H. Willers, and H. Paganetti, "Motion interplay as a function of patient parameters and spot size in spot scanning proton therapy for lung cancer," Int. J. Radiat. Oncol., Biol., Phys. **86**, 380–386 (2013).
[23]C. Bert, S. O. Grozinger, and E. Rietzel, "Quantification of interplay effects of scanned particle beams and moving targets," Phys. Med. Biol. **53**, 2253–2265 (2008).
[24]H. Shirato, Y. Seppenwoolde, K. Kitamura, R. Onimura, and S. Shimizu, "Intrafractional tumor motion: Lung and liver," Semin. Radiat. Oncol. **14**, 10–18 (2004).
[25]H. H. Liu, P. Balter, T. Tutt, B. Choi, J. Zhang, C. Wang, M. Chi, D. S. Luo, T. S. Pan, S. Hunjan, G. Starkschall, I. Rosen, K. Prado, Z. X. Liao, J. Chang, R. Komaki, J. D. Cox, R. Mohan, and L. Dong, "Assessing respiration-induced tumor motion and internal target volume using four-dimensional computed tomography for radiotherapy of lung cancer," Int. J. Radiat. Oncol., Biol., Phys. **68**, 531–540 (2007).